Experimental Demonstration of Real-Time High-Level QAM-Encoded Direct-Detection Optical OFDM Systems

Ming Chen, Jing He, Qirui Fan, Ze Dong, and Lin Chen

***Abstract*—In this paper, high-level quadrature amplitude modulation (QAM)-encoded real-time orthogonal frequency division multiplexing (OFDM) transceivers are implemented with two field programmable gate arrays and high-resolution digital-to-analog converter (DAC) and analog-to-digital converter (ADC). Some key digital signal processing (DSP) algorithms for real-time direct-detection optical OFDM (DDO-OFDM) system are presented and described in detail. To improve the effective number of bits of ADC and reduce quantization noise, the DAC operates at 5 GS/s with an oversampling factor of 2. Meanwhile, the optimal digital clipping ratio at the transmitter is also investigated by numerical simulation to optimize the performance of the real-time transmitter. The results show that the real-time measured BERs after 10-km SSMF are below the hard-decision forward error correction threshold of 3.8×10^{-3}. For comparison, the off-line BER performance is also analyzed using off-line DSP approaches. It shows that there is a negligible power penalty between the offline and real-time processing results. To the best of our knowledge, we have achieved the highest modulation format (1024-QAM) for real-time optical OFDM systems.**

***Index Terms*—Digital signal processing (DSP), high-level QAM modulation, orthogonal frequency division multiplexing (OFDM), real-time, spectral efficiency (SE).**

I. Introduction

RECENTLY, orthogonal frequency division multiplexing (OFDM) modulation technique has been proposed in high-speed fiber-optic transmission systems [1]–[3]. It is capable of compensating for chromatic dispersion and polarization-mode dispersion induced impairments by employing advanced and powerful digital signal processing (DSP)-enabled techniques, high spectral efficiency (SE) and single-tap frequency-domain equalization method. Among these OFDM-based systems, the intensity-modulated and direct-detection optical OFDM (IMDD-OOFDM) has been one of the candidate technologies for the second stage next generation PON (NG-PON2) [4], [5], due to its low complexity and cost-efficiency when compared with coherent optical OFDM (CO-OFDM) systems. Although time- and wavelength-division multiplexed PON (TWDM-PON) has been identified by full service access network (FSAN) as the primary solution for NG-PON2, it is based on the traditional on-off keying modulation with a very low SE. To further improve the SE, one of the most cost-effective approaches is to use OFDM-based systems with high-level M-ary quadrature amplitude modulation (M-QAM). By doing so, the electronic components' bandwidth requirement at both the transmitters and receiver can be reduced greatly. In [6], high-level QAM modulation formats such as 256-, 1024- and 2048-QAM have been applied into short-reach IMDD-OOFDM systems, in which the generation and reception of the electrical OFDM signals utilize off-line (OL) DSP approaches. However, computational precision and speed requirements have not been taken into account for practical DSP hardware implementations. Recently, some real-time (RT) OFDM transmitters or/and receivers have been experimentally demonstrated in IMDD optical transmission systems [7]–[14]. In our previous works [15], [16], a RT 7.19 Gb/s 256-, 64-, and 16-QAM adaptively modulated OFDM transceiver with an electrical SE of 5.76 bit/s/Hz, and a RT 5.55 Gb/s 1024-QAM OFDM transmitter with an electrical SE up to 8.88 bit/s/Hz are successfully demonstrated in the short-reach IMDD systems.

In this paper, we expand our previous work [16] in the demonstration of RT receiving 64-, 256-, 1024-QAM OFDM signal with an ADC over-sampling factor of 2. The 14-bit DAC at 2.5-GS/s and 10-bit ADC at 5-GS/s are used to generate and capture high-quality high-level QAM modulated OFDM signals, respectively. Meanwhile, a finite impulse response (FIR) digital filter is designed and implemented in the receiver to improve the signal-to-noise ratio (SNR) of the received OFDM samples. In addition, the optimal digital clipping ratio for different DAC resolutions is investigated by numerical simulation. The principles of some key DSP algorithms for RT direct-detection optical OFDM (DDO-OFDM) system, including single training sequence (TS)-based symbol timing synchronization and channel equalization, and QAM de-mapping are described in detail. Subsequently, the bit error rate (BER) performances of the RT 1024-, 256-, and 64-QAM optical OFDM signals at 5.55-, 4.44- and 3.33-Gb/s are investigated in short-reach IMDD-OOFDM systems, respectively. After 10 km SSMF transmission, the BER less than a hard-decision forward error correction (HD-FEC) threshold of 3.8×10^{-3} is successfully achieved with a

Manuscript received February 5, 2015; revised May 14, 2015; accepted July 14, 2015. Date of publication July 23, 2015; date of current version October 5, 2015. This work was supported by the National Natural Science Foundation of China under Grants 61307087 and 61377079, by the National "863" High Tech Research and Development Program of China (2011AA010203), and by the Fundamental Research Funds for the Central Universities and Young Teachers Program of Hunan University.

M. Chen, J. He, Q. Fan, and L. Chen are with the Key Laboratory for Micro/Nano Optoelectronic Devices of Ministry of Education, College of Computer Science and Electronic Engineering, Hunan University, Changsha 410082, China (e-mail: jhe@hnu.edu.cn).

Z. Dong is with the Department of Electronics Science and Technology, Huaqiao University, Xiamen 361021, China.

Color versions of one or more of the figures in this paper are available online at http://ieeexplore.ieee.org.

Digital Object Identifier 10.1109/JLT.2015.2458012

negligible power penalty for all of high-level QAM modulated optical OFDM systems.

This paper is organized as follows. In Section II, the principle of the RT DDO-OFDM systems and the TS generation method are presented. In Section III, the optimal digital clipping ratio is studied by simulation. In Section IV, we introduce some key DSP algorithms that are used in the experiment. The experimental setup of RT high-level QAM-encoded optical OFDM short-reach transmission systems is described in Section V. In Section VI, we discuss the experimental results. Finally, the conclusions are drawn in Section VII.

II. Theoretical Analysis

In this section, the principle of the Mach–Zehnder modulator (MZM)-based optical direct-detect OFDM systems is firstly introduced. It is very important to understand why we design the TS in that way.

After the MZM, the output intensity-modulated and double side-band optical OFDM signal can be expressed as [17]

$$E_o(t) = \sqrt{P_0}\cos\left(\frac{\pi(V_{\rm dc}+v_m(t))}{2V_\pi}\right)e^{j(2\pi f_0 t+\varphi_0)} \quad (1)$$

where P_0,f_0 and φ_0 are the output optical power, center frequency and initial phase of continuous-wave laser, respectively. The MZM is characterized by its half-wave voltage V_π, and is biased by $V_{\rm dc}$. $v_m\,(t)$ is the modulated signal.

For simplicity, the effects of fiber optic link are ignored. After optical-to-electrical conversion (O/E), the output current $i_{\rm out}\,(t)$ of the photodiode with a responsivity of γ is calculated by squaring $E_0\,(t)$, then

$$\begin{aligned} i_{\rm out}\,(t) &= \gamma\,|E_o(t)|^2 \\ &= \frac{P_0}{2}\gamma\left\{1+\cos\left(\frac{\pi V_{\rm dc}}{V_\pi}+\frac{\pi v_m(t)}{V_\pi}\right)\right\} \\ &= \frac{P_0}{2}\gamma\left\{1+\cos\left(\frac{\pi V_{\rm dc}}{V_\pi}\right)\cos\left(\frac{\pi v_m(t)}{V_\pi}\right)\right. \\ &\quad \left.-\sin\left(\frac{\pi V_{\rm dc}}{V_\pi}\right)\sin\left(\frac{\pi v_m(t)}{V_\pi}\right)\right\}. \end{aligned} \quad (2)$$

When the MZM is biased at a quadrature point, i.e., $V_{\rm dc}=\pm V_\pi/2$, the Eq. (2) can be simplified as $i_{\rm out}\,(t)=\mp P_0/2\gamma\sin\left(\pi v_m\,(t)/V_\pi\right)+P_0/2\gamma$. Based on the Taylor series expansion with respect to $v_m\,(t)$, the expression is given by

$$\begin{aligned} i_{\rm out}\,(t) &= \frac{P_0}{2}\gamma \\ &\times\left\{1\mp\frac{\pi v_m(t)}{V_\pi}\pm\left(\frac{\pi v_m(t)}{V_\pi}\right)^3/3!\mp\left(\frac{\pi v_m(t)}{V_\pi}\right)^5/5!\pm\ldots\right\} \end{aligned} \quad (3)$$

From Eq. (3), the base-band OFDM signal can be recovered with a negligible high odd-order distortion if a small signal is used to drive the MZM.

For another special case, as $V_{\rm dc}=\pm V_\pi$ (the MZM is biased at null point (NP),$i_{\rm out}\,(t)=-P_0/2\gamma\cos\left(\pi v_m\,(t)/V_\pi\right)+P_0/2\gamma$ after Taylor series expansion, $i_{\rm out}\,(t)$ is expressed as

$$i_{\rm out}\,(t)=\frac{P_0}{2}\gamma\left\{\left(\frac{\pi v_m(t)}{V_\pi}\right)^2/2!-\left(\frac{\pi v_m(t)}{V_\pi}\right)^4/4!+\ldots\right\}. \quad (4)$$

Based on Eq. (4), as the MZM biased at NP, the useful signal $v_m\,(t)$ cannot be recovered after directly detected by a photodiode. Besides, if $v_m\,(t)$ is a small signal, the second item in Eq. (4) regarded as signal-to-signal beating interference (SSBI) is dominant.

For the cases of $V_{\rm dc}\neq\pm V_\pi/2$ or $\pm V_\pi$, according to the Eq. (2), $i_{\rm out}\,(t)$ includes useful signal $v_m\,(t)$as well as high-order distortions. And the degraded system performance is mainly attributed to SSBI among these high-order distortions.

In the practical applications, the SSBI may be introduced into received OFDM signal after O/E conversion. This fact is due to the problems of non-ideal power transfer function and DC bias offsets of MZM. To achieve an accurate channel estimation, a novel TS structure design method has been proposed in our previous works [18], [19], it is similar to that of Schmidl's [20] where the two halves of TS are made identical in time order by only transmitting a PN sequence on the even SCs. The TS is generated by modulating the odd SCs with BPSK symbols, while the even SCs are filled with zeros. In this paper, in order to maintain approximately constant signal energy for each symbol, the normalized BPSK symbols that modulated on the odd SCs are multiplied by $\sqrt{2}$ at the transmitter. All of data on the SCs are constrained to have Hermitian symmetry, and then result of IFFT will produce the real-valued time-domain TS, as shown in Fig. 1. In this way, after O/E conversion, the accurate channel estimation without SSBI can be obtained by utilizing one-tap frequency-domain estimation and interpolation methods. It should be noted that the modulated symbol on the odd SC of data-carrying OFDM signal still suffers from SSBI, but the accurate channel estimation can improve the system BER performance, especially for the high-level QAM modulated OFDM systems.

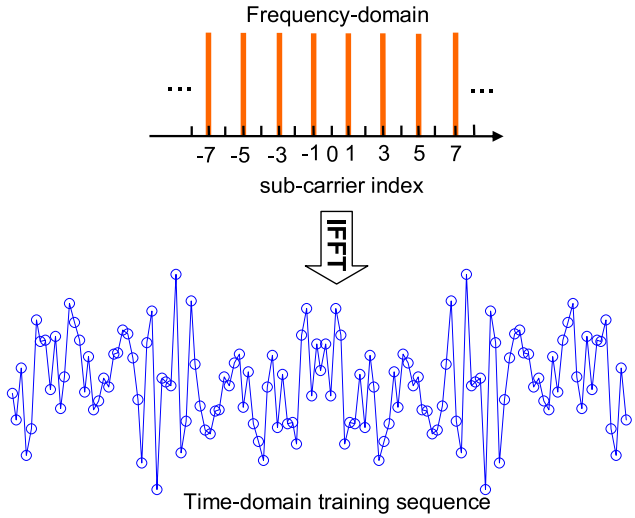

Fig. 1. The principle diagram of the TS generation.

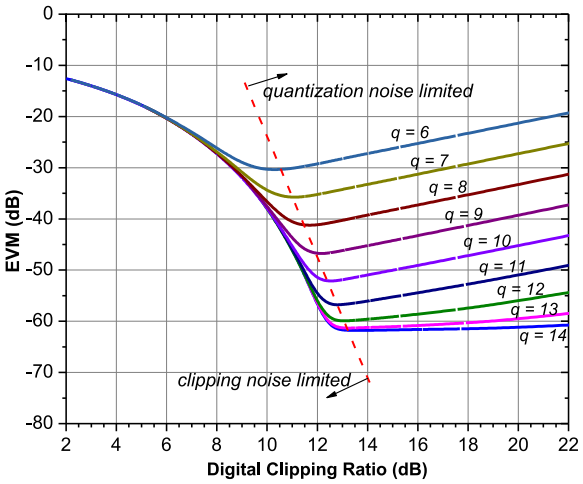

Fig. 2. Simulated EVM performance versus digital clipping ratio.

III. Digital Clipping

Due to the finite dynamic amplitude range or resolution of DAC, the output signal after IFFT should be digitally clipped at an optimal clipping ratio so as to obtain the best balance between the digital signal clipping and quantization noise. For a given digital clipping ratio $\zeta = 20 * \log_{10}(A/\mathrm{rms}[x(n)])$ in decibel, the clipped signal has the form as

$$y(n) = \begin{cases} -A, & ax(n) < -A \\ ax(n), & a|x(n)| \le A \\ A, & ax(n) > A \end{cases} \tag{5}$$

where $x(n)$ is the sample after IFFT process, $A$is the clipping threshold value, for a q-bit DAC, $A = 2^{q-1} - 1$. $\mathrm{rms}[x(n)]$ is the root mean square value of $x(n)$, a is a positive-valued scaling factor.

For different limited DAC bit resolutions, the relationship between error vector magnitude (EVM) performance of the clipped signal and digital clipping ratio is investigated by numerical simulation, and the related results are presented in Fig. 2.

As we can see clearly from Fig. 2, the optimal clipping ratio varies with the limited DAC resolution. For a specific DAC resolution, when clipping ratios are smaller than the optimal value, the peak-to-average power ratio of the un-clipped signal is relatively large, so the signal is clipped considerably, resulting in large clipping noise and deteriorated EVM performance. In addition, as the clipping ratios are larger than the optimal value, the value of $\mathrm{rms}[x(n)]$is relatively small. It equates to the clipped signal is quantized by a lower resolution DAC. Thus, the EVM performance is degraded mainly due to the quantization noise.

IV. RT DSP Algorithms

In the RT DDO-OFDM systems, some key DSP algorithms in the base-band transceiver are very important for a successful hardware implementation. These algorithms are described in detail as follows: At the receiver, to recover information-bearing bits from received OFDM samples, the TS-based symbol (or FFT windows) timing synchronization and channel equalization, and QAM de-mapping are performed on the receiver FPGA. It should be mentioned that, for simplicity, a common clock is used to drive both DAC and ADC, so that the effects of the sampling clock frequency offset (SCFO) can be avoided. Besides, a pilot-based SCFO estimation and compensation algorithm has been experimentally investigated in asynchronous systems [21], [22].

A. Symbol Timing Synchronization

In [23], cross-correlation algorithm can provide better performance at low SNR due to the averaging process of the correlator. For the real-valued IFFT/FFT based DDO-OFDM systems, there is no carrier frequency offset. Thus, the symbol timing synchronization can be implemented by calculating the cross-correlation between a local TS and received signal. The timing metric (TM) can be expressed as

$$M(d) = \sum_{n=0}^{N_{\mathrm{total}}} t(n) \cdot r(n+d) \tag{6}$$

where $t(n)$ is the transmitted TS with the length of $N_{\mathrm{total}} = N + N_{\mathrm{cp}}$, N and N_{cp} are IFFT/FFT size and the length of cyclic prefix, respectively. $r(n)$ is the received signal. The beginning of the TS can be estimated by searching the sample index d to maximize the $M(d)$ in Eq. (6).

According to the Eq. (6), the hardware implementation of the symbol timing synchronization based on the cross-correlation, which requires N_{total} real-valued multiplications and $N_{\mathrm{total}} - 1$ real-valued additions. For the high-speed optical communication systems, parallel data processing technique is necessary to reduce the FPGA operating frequency. By using the auto-correlation based synchronization methods, it can be implemented more efficiently by utilizing the iterative formula of the correlation function. However, the cross-correlation based synchronization can be implemented with a significant hardware cost. For a given number of parallel channels N_p, the required processing resource in this parallel implementation is estimated as $N_p N_{\mathrm{total}}$ real multipliers and $N_p(N_{\mathrm{total}} - 1)$ real adders.

Thus, in this paper, simplified synchronization for hardware-efficient implementation is proposed to reduce the demand of hardware resources. Only the sign bit of received samples is used to calculate the TM. And it can be defined as

$$\begin{aligned} M_{\mathrm{pro1}}(d) &= \overbrace{\sum_{n=0}^{N_{\mathrm{total}}-1} \mathrm{sign}[t(n)] \odot \mathrm{sign}[r(n+d)]}^{\text{The number of } \mathrm{sign}[t(n)] = \mathrm{sign}[r(n+d)]} \\ &\quad - \overbrace{\left(N_{\mathrm{total}} - \sum_{n=0}^{N_{\mathrm{total}}-1} \mathrm{sign}[t(n)] \odot \mathrm{sign}[r(n+d)]\right)}^{\text{The number of } \mathrm{sign}[t(n)] \neq \mathrm{sign}[r(n+d)]} \\ &= 2 \sum_{n=0}^{N_{\mathrm{total}}-1} \mathrm{sign}[t(n)] \odot \mathrm{sign}[r(n+d)] - N_{\mathrm{total}} \end{aligned} \tag{7}$$

$$d_{s1} = \arg\{M_{\mathrm{pro1}}(d) > \mathrm{Th}\} \tag{8}$$

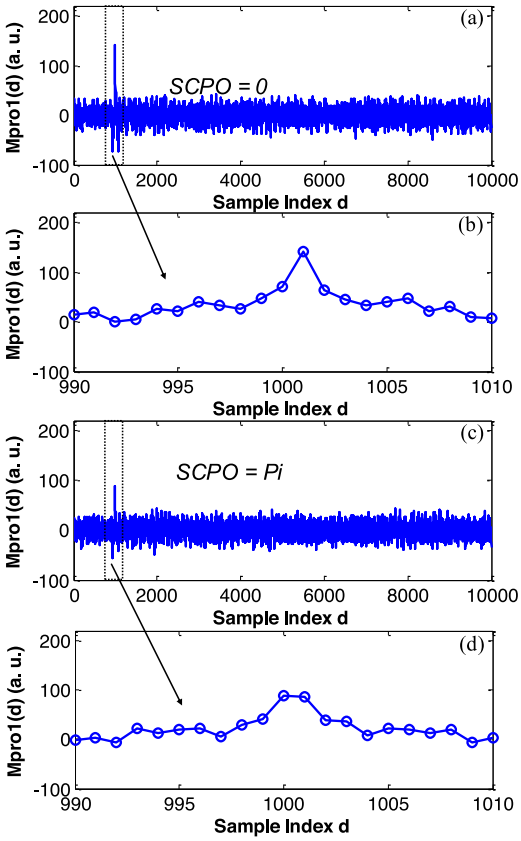

Fig. 3. Timing metric $M_{\mathrm{Pro1}}(d)$ with or without SCPO ($N = 128$, $N_{\mathrm{cp}} = 16$).

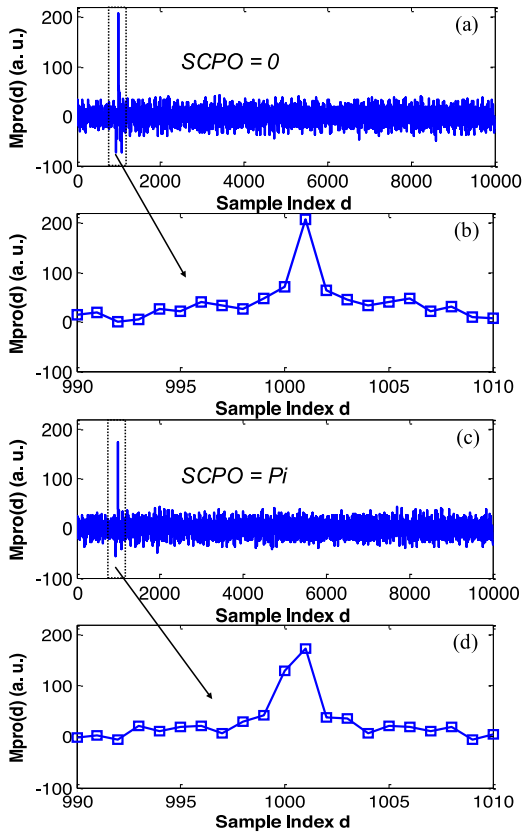

Fig. 4. Timing metric $M_{\mathrm{Pro}}(d)$ with or without SCPO ($N = 128, N_{\mathrm{cp}} = 16$, $V = 70$).

where $\mathrm{sign}[\cdot]$ stands for sign bit extractor, and it outputs a logic "0" for a positive number and "1" for a negative number. $\odot$ which is the XNOR operator. The starting point of the TS can be estimated by searching the sample to make the timing metric $M_{\mathrm{Pro1}}(d)$ larger than a threshold value TH. In this way, only sign-quantized signals are used to calculate the timing metrics, which greatly reduce computational complexity since it does not require multiplication or division operations, but logical operations and bits summation.

Because the effect of SCFO is small in short time, and symbol timing synchronization estimation occurs only in the first one TS, the effect of SCFO on the synchronization is negligible. However, the timing metric $M_{\mathrm{Pro1}}(d)$ is sensitive to the sampling clock phase offset (SCPO). The results obtained by simulation are shown in Fig. 3. The sharp peak of $M_{\mathrm{Pro1}}(d)$ is observed and the corresponding sample index d is the beginning of the TS in the absence of SCPO, as shown in Fig. 3(a) and (b); when SCPO equals Pi, the peak amplitude of $M_{\mathrm{Pro1}}(d)$ is attenuated greatly and plotted in Fig. 3(c), which leads to a reduced noise tolerance.

As presented in Fig. 3(d), the two adjacent amplitudes of $M_{\mathrm{Pro1}}(d)$ around the correct timing position are still larger than other positions, so the timing metric for symbol timing synchronization should be modified as

$$M_{\mathrm{Pro}}(d) = \begin{cases} M_{\mathrm{pro1}}(d) + M_{\mathrm{pro1}}(d-1), & M_{\mathrm{pro1}}(d) > V \\ M_{\mathrm{pro1}}(d), & M_{\mathrm{pro1}}(d) \le V \end{cases} \tag{9}$$

where V is threshold value. It is used to determine the value of $M_{\mathrm{Pro}}(d)$. The proposed symbol timing synchronization is capable of strong resistance to noise and SCPO. The simulated results are presented in Fig. 4.

The simplified symbol timing synchronization method can reduce hardware resources consumption, but synchronization performance is degraded due to the cross-correlation of only sign bits of received samples and a given TS. In addition, the variance of symbol timing offsets (STO) is larger than that of the traditional method in Eq. (6), which is mainly caused by the sum of two adjacent timing metrics and the threshold-decision search method for estimating the starting point of the TS. In fact, the SCPOs can also lead to the small STO within a sample period, even though Eq. (6) is used for symbol timing synchronization. In the OFDM system without cyclic suffix, the inter-channel interference maybe arises due to the STO. Hence, to solve this issue effectively, without increasing system overhead, the estimated optimal starting point d_s of the TS can be defined as

$$d_s = \arg\{M_{\mathrm{pro}}(d) > \mathrm{Th}\} - p = d_{s2} - p \tag{10}$$

where p is a positive integer within the range of $[0, N_{\mathrm{cp}}]$, and d_{s2} is estimated starting point, but it is not an optimal one. The optimal estimated starting point d_s can be obtained by moving d_{s2} toward the direction of CP with p samples. However, a suitable length of p should be chosen to maintain sufficient dispersion tolerance.

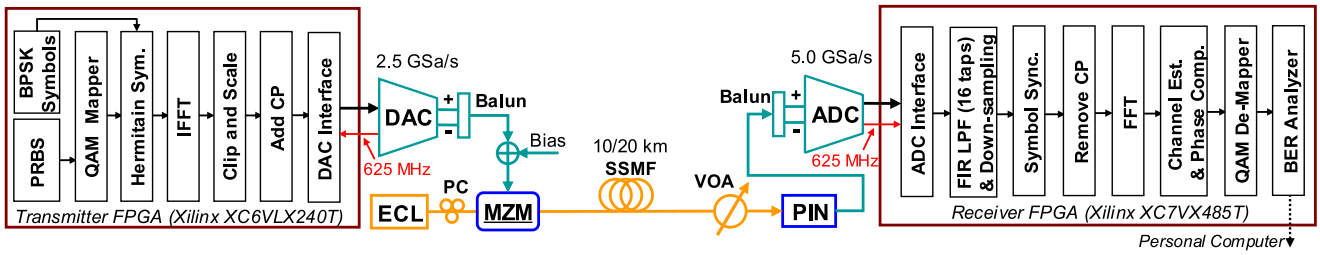

Fig. 5. Experimental setup of the RT DSP-based optical OFDM direct-detection system.

B. Channel Estimation

Once the symbol timing synchronization is completed, the samples in 16 parallel channels are reorganized and fed into FFT module. After the FFT, the output modulated symbols suffer from different attenuation and propagation delay. In addition, the STO can also be regarded as a part of channel response, and it can be compensated by channel equalization. In this paper, the TS can be used not only to realize symbol timing synchronization, but also to estimate channel response on data-carrying sub-carriers. Here, the TS-based channel estimation is divided into two steps. The first step is to estimate the channel responses on the odd SCs by using the simple single-tap frequency-domain estimation method, and it is written as

$$H\left(k_{\text{odd}}\right) = \frac{\text{TS}_{rv}\left(k_{\text{odd}}\right)}{\text{TS}_{\text{local}}\left(k_{\text{odd}}\right)} = \frac{1}{\sqrt{2}}\text{sgn}\left[\text{TS}_{\text{local}}\left(k_{\text{odd}}\right)\right]\cdot \text{TS}_{rv}\left(k_{\text{odd}}\right) \quad (11)$$

where $\text{TS}_{rv}\left(k_{\text{odd}}\right)$ and $\text{TS}_{\text{local}}\left(k_{\text{odd}}\right)$ are the k_{odd} th frequency component of the received and local known TS, respectively. k_{odd} is positive odd number. sgn[·] is the signum function of a real number.

After the estimated channel responses on the odd SCs are given, the channel responses on the even SCs$H\left(k_{\text{even}}\right)$ can be estimated by a simple linear interpolation method. In this way, the channel responses on the all of SCs$H\left(k\right)$ are estimated by the two-step estimation method.

C. Phase Compensation

For the traditional channel compensation method, the compensated symbol $R_c\left(k\right)$ is obtained by dividing received symbol $R\left(k\right)$ with the corresponding channel response $H\left(k\right)$. In this way, both the amplitude and phase response on the SCs can be compensated. The expression is given by

$$R_c(k) = \frac{R(k)}{H(k)} = \frac{R(k)H^*(k)}{|H(k)|^2} = \frac{\sqrt{2}\,\text{sgn}\left[\text{TS}_{\text{local}}\left(k\right)\right]\cdot R(k)\cdot \text{TS}^*_{rv}\left(k\right)}{\left|\text{TS}_{rv}\left(k\right)\right|^2}. \quad (12)$$

In this paper, to avoid the complex division operations for channel compensation, only the phase response on the modulated SCs is compensated, i.e., only the part of numerator of Eq. (12) $\text{sgn}\left[\text{TS}_{\text{local}}\left(k\right)\right]\cdot R(k)\cdot \text{TS}^*_{rv}\left(k\right)$ is implemented in the channel equalization stage; while the effects of amplitude response will be taken into account in the QAM de-mapper.

D. QAM De-Mapping

The hard-decision demodulation is used in QAM de-mapper. The decision threshold is defined as Thv. From Eq. (12), the hard-decision demodulation formula for m-QAM can be expressed as [24]

$$R_c(k) = \frac{\sqrt{2}\,\text{sgn}\left[\text{TS}_{\text{local}}\left(k\right)\right]\cdot R(k)\cdot \text{TS}^*_{rv}\left(k\right)}{\left|\text{TS}_{rv}\left(k\right)\right|^2} > Thv \quad (13)$$

To achieve m-QAM demodulation in our receiver, the formula for m-QAM demodulation is modified and given by

$$\text{sgn}\left[\text{TS}_{\text{local}}\left(k\right)\right]\cdot R(k)\cdot \text{TS}^*_{rv}\left(k\right) > \frac{1}{\sqrt{2}}\left|\text{TS}_{rv}\left(k\right)\right|^2\cdot Thv. \quad (14)$$

Based on an equivalent m-QAM demodulation method in Eq. (14), the channel equalization can be implemented in a hardware-efficient way.

V. Experiment Setup

The experimental setup of the FPGAs-based base-band 1024 (256/64)-QAM-encoded IMDD-OOFDM transmission system are shown in Fig. 5. A pseudo-random binary sequence (PRBS) with a length of 327 680 bits is firstly stored in read only memory (ROM) of the FPGA. It is used to assess the transmission performance of the RT systems. Meanwhile, a PN sequence including BPSK symbols is utilized to generate a TS for symbol timing synchronization and channel estimation. The DSP flow of the transmitter is as follows: Firstly, a parallel 320 (256/192)-bit sequence is fed into 32 1024 (256/64)-QAM mappers. In this paper, the 5th-36th sub-carriers (SCs) are modulated by 1024 (256/64)-QAM complex-valued symbols, while direct-current (DC) with the SC index of 0, Nyquist SCs (SC index is 64), and the other 31 positive-frequency SCs (SC indices from 1 to 5 and 37 to 63) are set zeros. Here, the 4 low-frequency zero-SCs are used to avoid serious sub-carrier to sub-carrier beating interference (SSBI) due to the square-law detector [15], and 27 high-frequency zero-SCs are used for over-sampling. In addition, 63 negative-frequency SCs (SC indices from -1 to -63) are the complex conjugates of the 63 corresponding positive-frequency SCs (SC indices from 1 to 63). After 14-bit fixed-point and 128-point IFFT process, the outputs are clipped at an optimal digital clipping ratio of 12.5 dB, and scaled so that it can be suitable for the 14-bit DAC (ADI AD9739A). Subsequently, a 16-sample

cyclic prefix (CP) is appended to the beginning of every OFDM symbol. The DAC is clocked by an external 2.5 GHz clock source and feedbacks a 625 MHz clock to DAC interface module of the transmitter FPGA. Due to 16-parallel channel signal processing scheme is performed, the FPGA only operates at 156.25 MHz so as to achieve a sample rate of 2.5 GS/s. Here, an OFDM frame consists of only one 144-sample TS and 1024 OFDM symbols. The TS-based symbol synchronization and channel estimation overhead $(144/(1025*144)*100\% \approx 0.1\%)$ is negligible. The OFDM frame duration is 59.04 μs $(1025*144*0.4\text{ns} = 59.04\ \mu\text{s})$, and the bandwidth of the RT OFDM signal is 625 MHz $(32/64*1250\text{MHz} = 625\text{MHz})$. For 1024-QAM modulation scheme, the net data rate is 5.55 Gb/s $(320*1024/(1025*144*0.4)$ Gb/s $\approx$ 5.55 Gb/s). Hence, the electrical SE is up to 8.88 b/s/Hz (5.55/0.625 b/s/Hz = 8.88 b/s/Hz).

The 2.5-GS/s balanced OFDM analog signal is firstly converted into unbalanced one by a balun. Then the single-ended OFDM signal with a peak-to-peak voltage of ~700 mV and 2.3 V DC bias are combined in a bias tee. To generate the intensity-modulated optical OFDM signal, the combined signal drives a LiNbO3 MZM with a half-wave voltage of 3.5 V, and a tunable external cavity laser is used as optical source at the transmitter. It should be mentioned that the MZM is sensitive to polarization, so a polarization controller is used in front to allow the correct polarization. After the MZM, the double-sideband optical OFDM signal with an optical power of 5.7 dBm is coupled into short-reach SSMF links. The dispersion coefficient and attenuation of the SSMF are 17 ps/nm/km and 0.19 dB/km, respectively. At the receiver, a variable optical attenuator with an insertion loss less than 1 dB is applied to change received optical power (ROP). The received optical signal is directly detected by a DC coupled PIN photo-diode with a bandwidth of 10 GHz, and converted to the real-valued base-band OFDM signal. The DC component of PIN output signal is removed by the second balun. It is also used to convert the single-ended OFDM signal to differential one. The differential analog signal is sampled by the 10-bit ADC at a sample rate of 5 GS/s. To avoid SCFO between the transmitter and receiver, it should be noted that a common 2.5 GHz clock is used for the DACs and ADCs. After analog-to-digital conversion, the 5 GS/s samples and a 625 MHz clock are fed to the FPGA. In the receiver, the key DSP functions including the FIR based low-pass filter (LPF) and down-sampling at a ratio of 2:1, TS-based symbol synchronization, 16-bit fixed-point and 128-point FFT, channel equalization, and 1024(256/64)-QAM de-mapping. For comparison purpose, the ADC captured samples are also analyzed by using OL DSP approaches.

VI. Results and Discussion

A. FIR Filter

To reduce the ADC quantization noise and improve the effective number of bits (ENOB) of the ADC, the ADC operates at 5 GS/s with an over-sampling factor of 2. The measured ENOBs of the ADC card over frequencies are listed as follows: 7.88 bit at 160 MHz, 6.98 bit at 1.2 GHz, and 6.46 bit at 2.2 GHz.

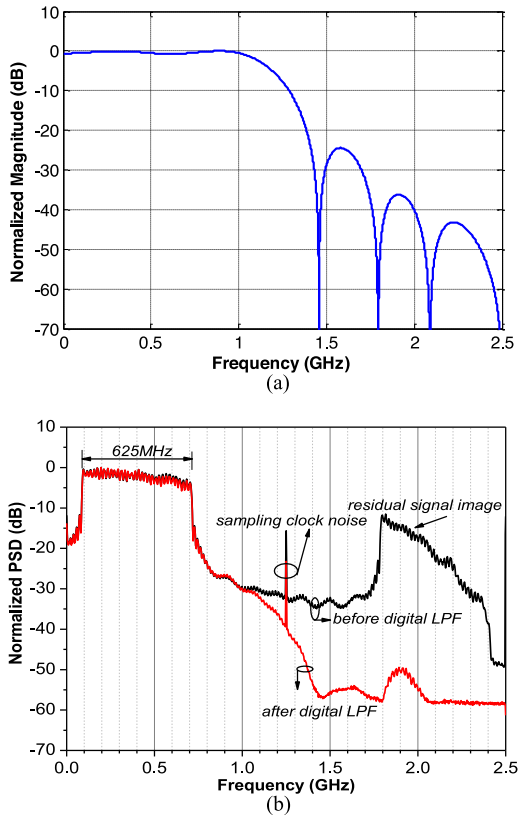

Fig. 6. (a) The normalized magnitude response of the designed FIR filter and (b) estimated normalized PSDs before/after the digital LPF.

In addition, in the receiver, a 16-tap FIR LPF is designed and implemented to suppress residual image interference. The corresponding filter coefficients are [−10 −12 18 20 −33 −40 80 224 224 80 −40 −33 20 18 −12 −10]. The normalized magnitude response of the digital filter is analyzed and shown in Fig. 6(a). The normalized power spectral densities (PSDs) of both unfiltered (black line) and filtered (red line) OFDM samples are given in Fig. 6(b). As we can see clearly from it, the band-width of the base-band OFDM signal is 625 MHz, and the image can be suppressed clearly (>40 dB) after passing through the FIR LPF. There is also a sampling clock-induced noise at 1.25 GHz, and the reason has been experimentally investigated in our previous works [15], [16]. The outputs of digital LPF are truncated to 10-bit fixed-point numbers for symbol timing synchronization module.

B. Electrical Back-to-Back Performance

In the electrical back-to-back (EBTB) configuration, the estimated channel response including amplitude and phase responses versus SC index are shown in Fig. 7(a). The maximum power fading on the SCs is about 7 dB. It is mainly attributed to the low-pass filtering effects of the electrical devices such as DAC roll-off, analog front-ends of DAC and ADC cards, etc. Moreover, the different phase response over SC is due to the SCFO between the DAC and ADC, as well as the STO caused by the proposed symbol timing synchronization. After the TS-based channel equalization, the error bits distribution

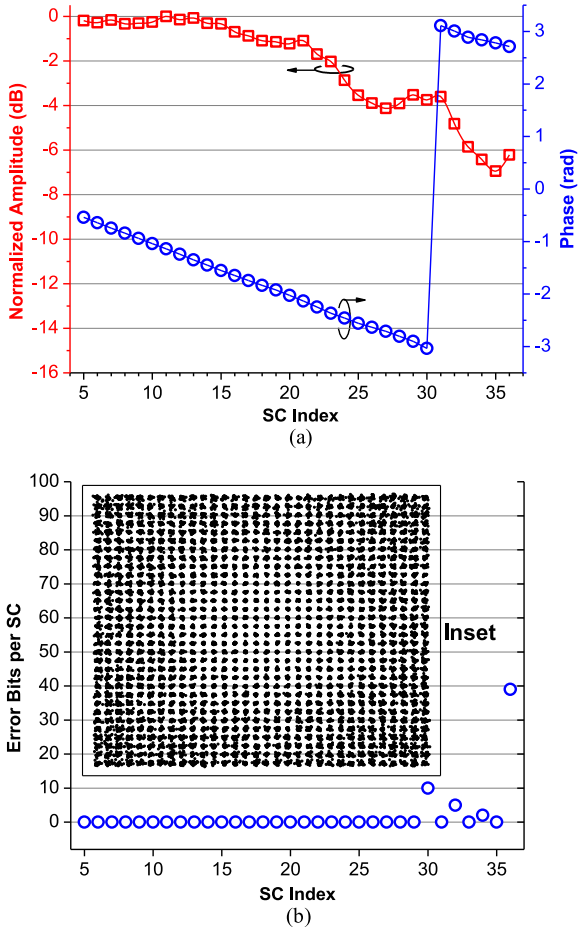

Fig. 7. (a) Estimated channel response and (b) OL error bits distribution and 1024-QAM constellation at EBTB case.

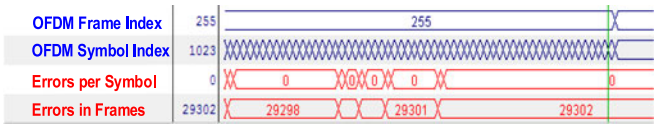

Fig. 8. RT recorded error bits in every OFDM symbols and 256 OFDM frames by Xilinx Analyzer.

and 1024-QAM constellation diagram by OL DSP are shown as inset in Fig. 7(b). The error bits are mainly located on the high-frequency SCs with high power fading. And the corresponding BER and error vector magnitude (EVM) are 1.71×10^{-4} and -37.5 dB, respectively. The RT EBTB BER performance by Xilinx ChipScope Pro tools is also illustrated in Fig. 8. The ranges of received OFDM symbol index and OFDM frame index are from 0 to 1,023 and 0 to 255, respectively. Meanwhile, the number of error bits in a certain OFDM symbol and number of error bits in received OFDM frames are also given in Fig. 8 for BER analysis. In this paper, BER is obtained by direct error bit counting over 256 OFDM frames, which contains 1,024 OFDM symbols per frame with a total of 83 886 080 bits. Here, the number of total error bits in the continuous recorded 1024 OFDM frames is 29302. Thus, the RT measured BER is $29,302/(320 * 256 * 1,024) = 3.49 \times 10^{-4}$.

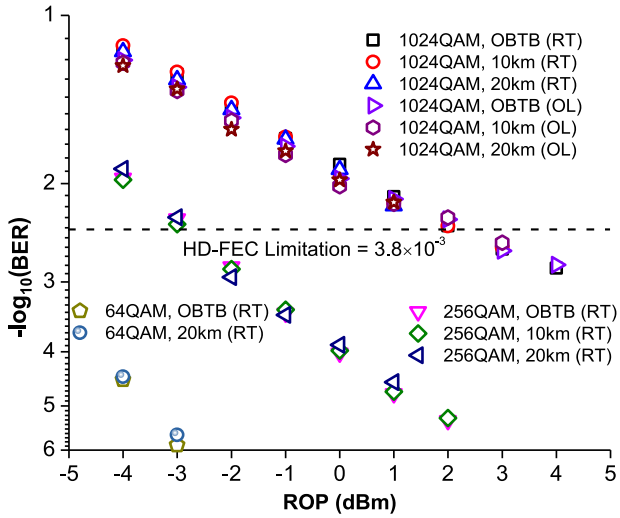

Fig. 9. RT and OL measured BER performances versus ROP.

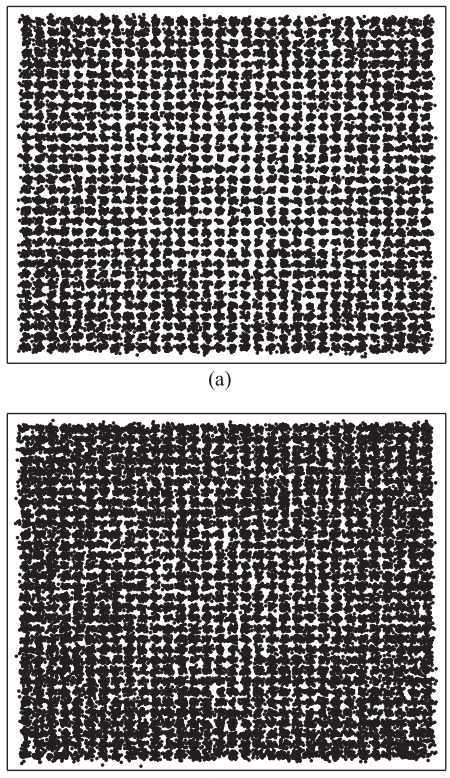

Fig. 10. The 1024-QAM constellation diagrams obtained by OL DSP approaches: (a) OBTB and ROP $= 4$ dBm, and (b) 20-km SSMF transmission and ROP $= 1$ dBm.

C. End-to-End 10/20 km SSMF Transmission Performance

The end-to-end transmission performances over SSMF links are shown in Fig. 9. After 10 and 20 km SSMFs transmission, the power penalties for both RT and OL DSP approaches are negligible. Compared with OL BER results, the RT BER performance is slightly degraded, which is mainly due to the limitation of computational precision. It should be mentioned that only one OFDM frame is used to analyze the BER

performance when using OL approaches, hence, it also may be a reason for the BER difference between RT and OL results. The RT measured BER after 10-km SSMF is below than the HD-FEC threshold of 3.8×10^{-3} [6]. For comparison, 256- and 64-QAM-encoded RT OFDM signals are generated and demodulated by re-configuring the FPGAs at the transceiver. At a BER of 3.8×10^{-3}, the required ROPs of 64-, 256- and 1024-QAM-encoded optical IMDD-OOFDM systems are less than -4, -3 and 2 dBm, respectively. The degraded BER performances over decreased ROPs are mainly attributed to the ADC quantization noise and photo-diode noise. Therefore, the receiver sensitivity can be further improved by using a suitable linear RF amplifier or high-sensitivity APD photo-detector [25], or optimizing optical carrier-to-signal power ratio (CSPR) [26], [27]. The OL 1024-QAM constellations for optical back-to-back (OBTB) and post-20 km SSMF are shown in Fig. 10(a) and (b), respectively.

VII. Conclusion

In the paper, the high-level QAM-encoded RT OFDM transceivers were successfully implemented with two off-the-shelf FPGAs, 14-bit 2.5 GS/s DAC and 10-bit 5 GS/s ADC. Meanwhile, the transceivers were experimentally investigated in short-reach direct-detection transmission systems. Some key DSP algorithms for RT DDO-OFDM transmission systems have been presented. In addition, in order to obtain the best balance between the digital signal clipping and quantization noise, the optimal digital clipping ratio for the transmitter was studied by numerical simulation. The BER below the HD-FEC threshold of 3.8×10^{-3} after 10 km SSMF was achieved without power penalty for all of RT high-level QAM-encoded systems. Moreover, there is a negligible power penalty between the OL and RT BER results.

References

[1] W. Shieh and C. Athaudage, "Coherent optical orthogonal frequency division multiplexing," *Electron. Lett.*, vol. 42, no. 10, pp. 587–589, 2006.

[2] J. Armstrong, "OFDM for optical communications," *J. Lightw. Technol.*, vol. 27, no. 3, pp. 189–204, Feb. 2009.

[3] D. Qian, E. Ip, M.-F. Huang, M.-J. Li, and T. Wang, "698.5-Gb/s PDM-2048QAM transmission over 3 km multicore fiber," presented at the 39th Eur. Conf. Exhib. Opt. Commun., London, U.K., 2013, Paper Th.1.C.5.

[4] Y. Luo, X. Zhou, F. Effenberger, X. Yan, G. Peng, Y. Qian, and Y. Ma, "Time- and wavelength-division multiplexed passive optical network (TWDM-PON) for next-generation PON stage 2 (NG-PON2)," *J. Lightw. Technol.*, vol. 31, no. 4, pp. 587–593, Feb. 2013.

[5] R. Giddings, "Real-time digital signal processing for optical OFDM-based future optical access networks," *J. Lightw. Technol.*, vol. 32, no. 4, pp. 553–570, Feb. 2014.

[6] F. Li, X. Li, L. Chen, Y. Xia, C. Ge, and Y. Chen, "High-Level QAM OFDM system using DML for low-cost short reach optical communications," *IEEE Photon. Technol. Lett.*, vol. 26, no. 9, pp. 941–944, May 2014.

[7] E. Hugues-Salas, Q. Zhang, R. P. Giddings, M. Wang, and J. Tang, "Adaptability-enabled record-high and robust capacity-versus-reach performance of real-time dual-band optical OFDM signals over various OM1/OM2 MMF systems [invited]," *IEEE/OSA J. Opt. Commun. Netw.*, vol. 5, no. 10, pp. A1–A11, Oct. 2013.

[8] Y. Benlachtar, P. M. Watts, R. Bouziane, P. A. Milder, R. J. Koutsoyannis, J. C. Hoe, M. Püschel, M. Glick, and R. I. Killey, "Real-time digital signal processing for the generation of optical orthogonal frequency-division-multiplexed signals," *IEEE J. Sel. Topics Quantum Electron.*, vol. 16, no. 5, pp. 1235–1244, Sep./Oct. 2010.

[9] S.-H. Cho, K. W. Doo, J. H. Lee, J. Lee, S. I. Myong, and S. S. Lee, "Demonstration of a real-time 16 QAM encoded 11.52 Gb/s OFDM transceiver for IM/DD OFDMA-PON systems," presented at the 18th Opt. Electron. Commun. Conf., Kyoto, Japan, 2013, Paper WP2-3.

[10] F. Li, X. Xiao, X. Li, and Z. Dong, "Real-time demonstration of DMT-based DDO-OFDM transmission and reception at 50Gb/s," presented at the 39th Eur. Conf. Exhib. Opt. Commun., London, U.K., 2013, Paper P.6.13.

[11] N. Kaneda, Q. Yang, X. Liu, S. Chandrasekhar, W. Shieh, and Y.-K. Chen, "Real-time 2.5 GS/s coherent optical receiver for 53.3-Gb/s sub-banded OFDM," *J. Lightw. Technol.*, vol. 28, no. 4, pp. 494–501, Feb. 2010.

[12] Y. Qiao, J. Zhou, L. Wang, and Y. Ji, "1-Gb/s multimedia service upsignal transmission in real-time DSP-based OFDM-PON," in *Proc. IEEE/CIC Int. Conf. Commun. China*, 2013, pp. 190–194.

[13] N. Kaneda, T. Pfau, H. Zhang, J. Lee, Y.-K. Chen, C.-J. Youn, Y.-H. Kwon, E. S. Num, and S. Chandrasekhar, "Field demonstration of 100-Gb/s real-time coherent optical OFDM detection," presented at the European Conf, Optical Communication, Cannes, France, 2014, Paper Th.2.5.3.

[14] X. Q. Jin, R. P. Giddings, E. Hugues-Salas, and J. M. Tang, "Real-time demonstration of 128-QAM-encoded optical OFDM transmission with a 5.25bit/s/Hz spectral efficiency in simple IMDD systems utilizing directly modulated DFB lasers," *Opt. Exp.*, vol. 17, no. 22, pp. 20484–20493, 2009.

[15] M. Chen, J. He, J. Tang, X. Wu, and L. Chen, "Experimental demonstration of real-time adaptively modulated DDO-OFDM systems with a high spectral efficiency up to 5.76bit/s/Hz transmission over SMF links," *Opt. Exp.*, vol. 22, no. 15, pp. 17691–17699, 2014.

[16] M. Chen, J. He, and L. Chen, "Real-time demonstration of an FPGA-based 1024-QAM OFDM transmitter in short-reach IMDD systems," *IEEE Photon. Technol. Lett.*, vol. 27, no. 8, pp. 824–827, Apr. 2015.

[17] K.-P. Ho, *Phase-Modulated Optical Communication Systems*. New York, NY, USA: Springer, 2005, pp. 36–48.

[18] X. Wang, J. Yu, Z. Cao, J. Xiao, and L. Chen, "SSBI mitigation at 60 GHz OFDM-ROF system based on optimization of training sequence," *Opt. Exp.*, vol. 19, no. 9, pp. 8839–8846, 2011.

[19] W. Zou, J. Yu, and J. Xiao, "Direct-detection optical orthogonal frequency division multiplexing system with new training sequence," *Frequenz*, vol. 66, no. 1, pp. 27–32, 2012.

[20] T. M. Schmidl and D. C. Cox, "Robust frequency and timing synchronization for OFDM," *IEEE Trans. Commun.*, vol. 45, no. 12, pp. 1613–1621, 1997.

[21] M. Chen, J. He, J. Tang, and L. Chen, "Pilot-aided sampling frequency offset estimation and compensation using DSP technique in DD-OOFDM systems," *Opt. Fiber Technol.*, vol. 20, pp. 268–273, 2014.

[22] M. Chen, J. He, Z. Cao, J. Tang, L. Chen, and X. Wu, "Symbol synchronization and sampling frequency synchronization techniques in real-time DDO-OFDM systems," *Opt. Commun.*, vol. 326, pp. 80–87, 2014.

[23] A. Fort, J.-W. Weijers, V. Derudder, W. Eberle and A. Bourdoux. "A performance and complexity comparison of auto-correlation and cross-correlation for OFDM burst synchronization," in *Proc. Int. Conf. Acoust. Speech, Signal Process.*, vol. 2, pp. II-341–II-344, 2003.

[24] M. Chen, J. He, and L. Chen, "Real-time optical OFDM long-reach PON system over 100-km SSMF using a directly modulated DFB laser," *IEEE/OSA J. Opt. Commun. Netw.*, vol. 6, no. 1, pp. 18–25, Jan. 2014.

[25] Q. W. Zhang, E. Hugues-Salas, Y. Ling, H. B. Zhang, R. P. Giddings, J. J. Zhang, M. Wang, and J. M. Tang, "Record-high and robust 17.125 Gb/s gross-rateover 25 km SSMF transmissions of real-time dual-band optical OFDM signals directly modulated by 1 GHz RSOAs," *Opt. Exp.*, vol. 22, no. 6, pp. 6339–6348, 2014.

[26] A. Ali, J. Leibrich, and W. Rosenkranz, "Spectral efficiency and receiver sensitivity in direct detection optical-OFDM," presented at the Opt. Fiber Communication, San Diego, CA, USA, 2009, Paper OMT7.

[27] J. Ma, "Simple signal-to-signal beat interference cancellation receiver based on balanced detection for a single-sideband optical OFDM signal with a reduced guard band," *Opt. Lett.*, vol. 38, no. 21, pp. 4335–4338, 2013.

Authors' biographies not available at the time of publication.